A Magnetic Head Design for Manipulating Single Proteins with Force

Rafael Tapia-Rojo, Edward C. Eckels, and Julio M. Fernandez

Department of Biological Sciences, Columbia University, New York, NY 10027, USA

Abstract

Magnetic heads are ubiquitously used to record and read on magnetic tapes in technologies as diverse as old cassettes or VHS tapes, modern hard drive disks, or magnetic bands in credit/debit or subway cards. They are designed to convert electric signals into fluctuations on the magnetic field at very high frequencies, crucial for the high density storage which is demanded nowadays. Here, we twist this traditional use of magnetic heads and implement one in a new force spectrometer design, where the magnetic field is used to pull on proteins tethered to superparamagnetic beads. Our instrument offers the same features as magnetic tweezers—intrinsic force-clamp conditions, with accurate control of the force, and intrinsic stability—, but with the novel ability of changing the force instantaneously, which allows to investigate protein dynamics at very short timescales, or under arbitrary force signals. We calibrate our instrument by relying on Karlqvist approximation of the field created by a magnetic head—the first building block of magnetic recording theory—through the force scaling of the unfolding/folding step-sizes of protein L, used as a molecular template. This results in a force range between 0 and 50 pN, when working at distances above 250 μm, and electric currents up to 1 A. We illustrate the potential of our instrument by studying the folding mechanism of protein L upon ultra-fast force quenches. This allows us to describe that, in a short timescale of 50 ms, the unfolded protein L evolves to an

ensemble of weak collapsed states, eventually acquiring the native conformation in a timescale of seconds. Our instrumental development provides a unique capability of interrogating individual molecules under fast-changing force signals, which opens a range of novel force spectroscopy schemes of unexplored biological significance.

Magnetic head recording systems have been perfected over decades, resulting in a deep understanding of the physical features of magnetic heads, which evolved to create strong magnetic fields that can change very rapidly in time.[1,2] Hence, it becomes natural that we explore the use of this technology in its application to force spectroscopy. Indeed, magnetic tweezers force spectroscopy uses a magnetic field created by a pair of permanent magnets to apply pulling forces on biomolecules tethered to superparamagnetic beads.[3–7] Due to the extreme compliance of the magnetic trap, magnetic tweezers offer intrinsic force-clamp conditions and an exquisite control of the pulling force, which, combined with HaloTag covalent chemistry, provides an inherent stability, and gives access to very long timescales, of several hours or even days.[8–10] However, in magnetic tweezers, the force is changed by moving mechanically this pair of permanent magnets—commonly through a motor or a voice-coil actuator—, which is a slow process that takes up to 100 ms. This limitation impedes, for instance, to capture early molecular events that can occur upon fast force changes, or to apply alternative force protocols where the perturbation changes quickly in time, motivating the need to implement fast-changing magnetic fields.

In this Letter, we present a magnetic head tweezers force spectrometer, capable of changing the force in a micro-second timescale. As the mechanical force is controlled by the electric current which flows through the head core, it can be changed as fast as the current can be supplied. Using Kalqvist approximation of the magnetic field,[11] we calibrate our instrument by developing the analytical relationship between the applied force, and the electric current and vertical distance of the head to the magnetic bead through only two free parameters. We determine these parameters by fitting the extension of folding/unfolding steps of protein L at different currents and distances to the freely-jointed chain model. We prove the validity

of our calibration by using talin domain R3 and as a "force reporter", given its exquisite sensitivity to the pulling force.[12,13] To demonstrate the potential of our instrument, we explore the folding mechanism of protein L at very short timescales. By doing ultra-fast force quenches to 1 pN during varying times between 10 ms and 10 s, we observe that protein L progresses first into an immature weak intermediate—*molten globule*—in $\sim$ 50 millisecond, and eventually evolves to a far more mechanically stable native state over a timescale of few seconds.

Magnetic head tweezers follow the same scheme as conventional magnetic tweezers,[6] but substituting the pair of voice coil-mounted permanent magnets by a micro-positioned magnetic head (Brush Industries, 902836), identical to those employed in tape recorders or to read credit cards (Fig. 1A).[1] A magnetic head consists of a toroidal core of magnetic material with large permeability μ. The core has a narrow gap (25 μm in our case), so that, by supplying electric current to the coil wrapped around, a strong magnetic field is generated over the gap region (Fig. 1B). Compared to other electromagnetic tweezers designs[4,14,15]—which use typically narrow tips to pull on molecules or to trap and manipulate magnetic beads—our setup highlights the ability to change the force with a bandwidth of several kHz. In the same sense that magnetic heads are designed for converting electric signals into a magnetic record on a tape or wire, we employ it to convert electric signals into force signals, applied to tethered molecules (see Fig. 1B and C).

In magnetic tweezers, the applied force is determined by using a calibration curve that relates the pulling force with the vertical distance between the magnet and the paramagnetic bead.[4–6] This *magnet law* is specific for the geometry and strength of the magnets and the specifications of the magnetic beads—volume and magnetic composition. In our case, the pulling force depends, not only on the distance between the magnetic head and the bead, but also on the magnitude of the supplied current. Following the same strategy we developed previously,[6] we generate a *current law* by relating the pulling force F with the distance from the head to the bead z and the electric current I through the unfolding/folding step-sizes of

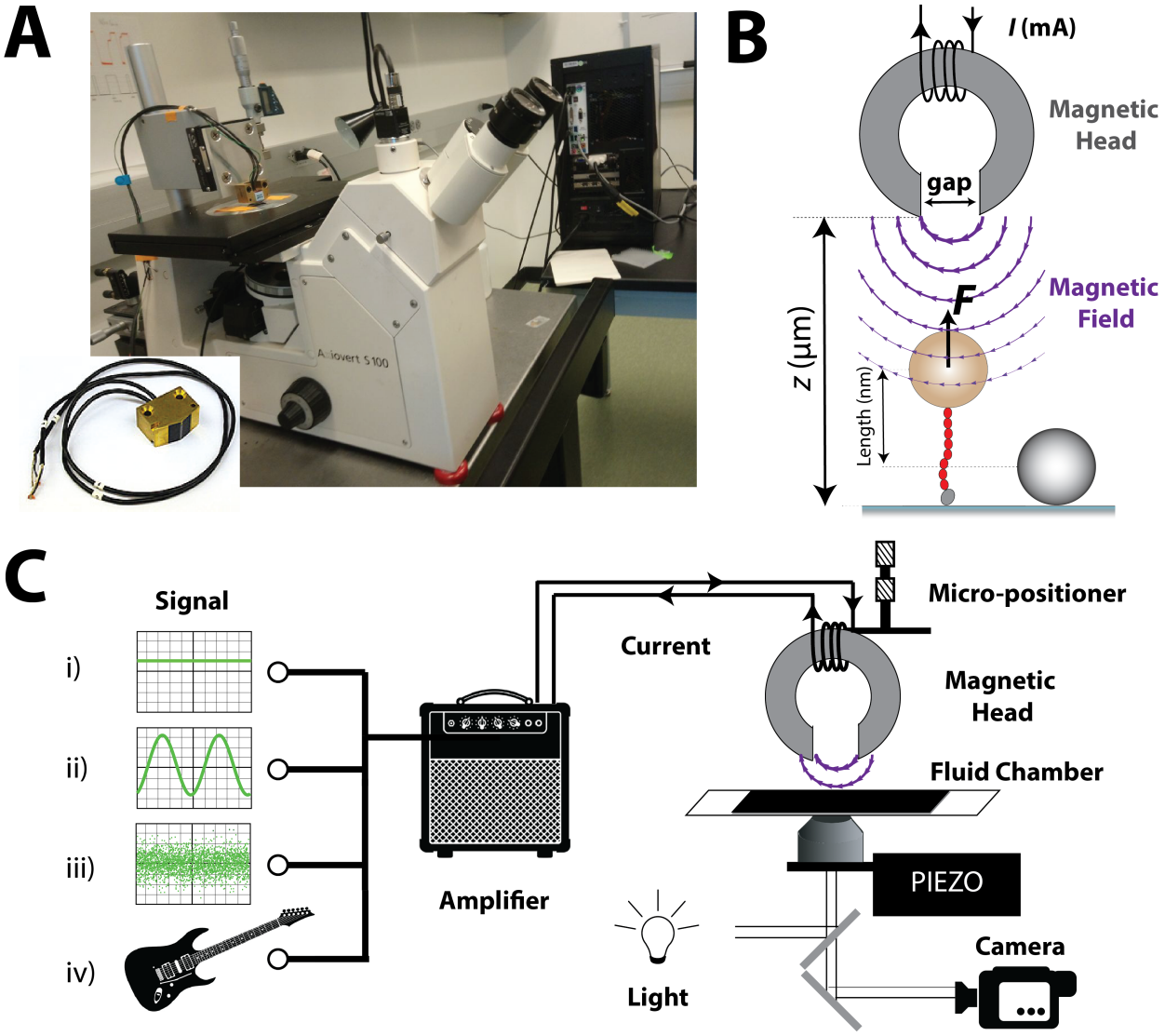

Figure 1: Magnetic head tweezers setup. (A) Picture of the magnetic head tweezers setup, with the magnetic head highlighted in the inset. (B) Schematics of the magnetic head tweezers experiment. The magnetic head generates a magnetic field over the gap region, applying a pulling force on the superparamagnetic bead. The polyprotein (red balls) is tethered to a glass coverslip by HaloTag chemistry, and to the bead though a streptavidin-biotin bond. (C) Schematics of the magnetic head tweezers setup. The magnetic head is precisely positioned over the fluid chamber, so that the force is controlled only by the electric current, which can be built by a combination of (i) constant, (ii) sinusoidal, (iii) noise, (iv) or any arbitrary signal. The electric signal is amplified and supplied to the head, which converts it to mechanical force. The remainder includes a piezo-mounted objective, an inverted microscope and a high-speed CCD camera.

protein L, which scale with the force following standard polymer models such as the freely-jointed chain model.[16] In order to address this problem, we need an analytical expression that relates the pulling force with these two magnitudes, z and I. For conventional magnetic tweezers an exponential dependence between force and distance has been assumed.[6] Here, we can derive an analytical expression for the current-distance relation, since the magnetic field created by a magnetic head can be well described by Karlqvist approximation:[1,11]

$$\begin{aligned} H_x &= \frac{H_g}{\pi}\left[\tan^{-1}\left(\frac{g/2+x}{z}\right)+\tan^{-1}\left(\frac{g/2-x}{z}\right)\right], \\ H_z &= -\frac{H_g}{2\pi}\log\frac{(g/2+x)^2+y^2}{(g/2-x)^2+y^2}, \end{aligned} \tag{1}$$

where H_x and H_z are the lateral and vertical components, respectively, g is the gap width, and $H_g = NI\eta/g$ the deep gap field, being N the number of turns around the head core, I the intensity of the current, and η the field efficiency, which is determined by the geometry of the head (see SI for further details). Now, the force acting on a superparamagnetic bead due to an applied magnetic field can be described as:[17]

$$\vec{F} = \frac{V\chi_{bead}}{\mu_0}\left(\vec{B}\cdot\nabla\right)\vec{B} + \rho V\nabla\left(\vec{M}_0\cdot\vec{B}\right), \tag{2}$$

where ρ is the density of the bead, V its volume, $\vec{M}_0$ the initial magnetization of the bead, $\vec{B}$ the applied magnetic field ($\vec{B} = \mu_0\vec{H}$ if we neglect the magnetic properties of the medium), χ_{bead} the initial magnetic susceptibility of the bead, and $\mu_0 = 4\pi\times10^{-7}$ TmA^{-1} the permeability of the vacuum. In the literature, this magnetic force is often assumed to consist solely on the first term $\vec{F} = \frac{V\chi_{bead}}{\mu_0}\left(\vec{B}\cdot\nabla\right)\vec{B}$. However, it has been demonstrated how in actual superparamagnetic beads, the initial magnetization $\vec{M}_0$ can be comparable to that induced by weak magnetic fields ($\vec{B}\sim mT$);[17] therefore Eq. 2 is more accurate to describe the magnetic force in the current and distance range we will be working on.

The lateral F_x and vertical F_z components of the magnetic force acting on the magnetic

bead can be obtained by combining Eqs. 2 and 1 (see SI). For practical reasons, it is convenient to work over the gap region ($-g/2 \leq x \geq g/2$), as the magnetic field is constant and the lateral component vanishes $F_x = 0$. Thus, the vertical component evaluated at $x \approx 0$ can be written as (we drop the z subscript):

$$F(z,I) = AI^2 \tan^{-1}\left(\frac{g/2}{z}\right) \frac{1}{1+\left(\frac{z}{g/2}\right)^2} + BI \frac{1}{1+\left(\frac{z}{g/2}\right)^2}, \tag{3}$$

where A and B are constants built by combining the physical parameters of our problem (see SI for their explicit expression). Our calibration strategy hinges on determining A and B by relating the extension ΔL of the folding/unfolding steps of protein L, used as a molecular ruler, with the pulling force F through the FJC model:

$$\Delta L(z,I) = \Delta L_c \left[\coth\left(\frac{F(z,I)l_K}{k_BT}\right) - \frac{k_BT}{F(z,I)l_K}\right], \tag{4}$$

where $F(z,I)$ takes the shape of Eq. 3, ΔL_c is the contour length increment, l_K the Kuhn length ($\Delta Lc = 16.3$ nm and $l_K = 1.1$ nm for protein L[8]), and $k_BT = 4.11$ pNnm the thermal energy. This dependence can also be described in terms of the worm like chain model, which produce equivalent results, being employed interchangeably. In our case, the freely jointed chain model is more convenient for analytical reasons.

We carry out experiments on protein L octamers as described previously,[6] working at different distances z and currents I, and measuring the average step-size $\Delta L(z,I)$ (see SI for a detailed methods section). Figure 2A shows a typical magnetic head tweezers trajectory for a protein L octamer. First, working at a distance of $z = 275$ μm, we unfold the octamer with a pulse of 800 mA, where each domain unfolding appears as a stepwise increase in the extension of 14.3 nm. Next, we decrease the current to 225 mA, and the polyprotein collapses, showing unfolding/refolding kinetics with upward and downward steps of 7.9 nm, respectively. Finally, we unfold the remaining domains at 665mA, and move the head away from the bead to a distance of $z = 550$ μm, which results in a great decrease of the pulling

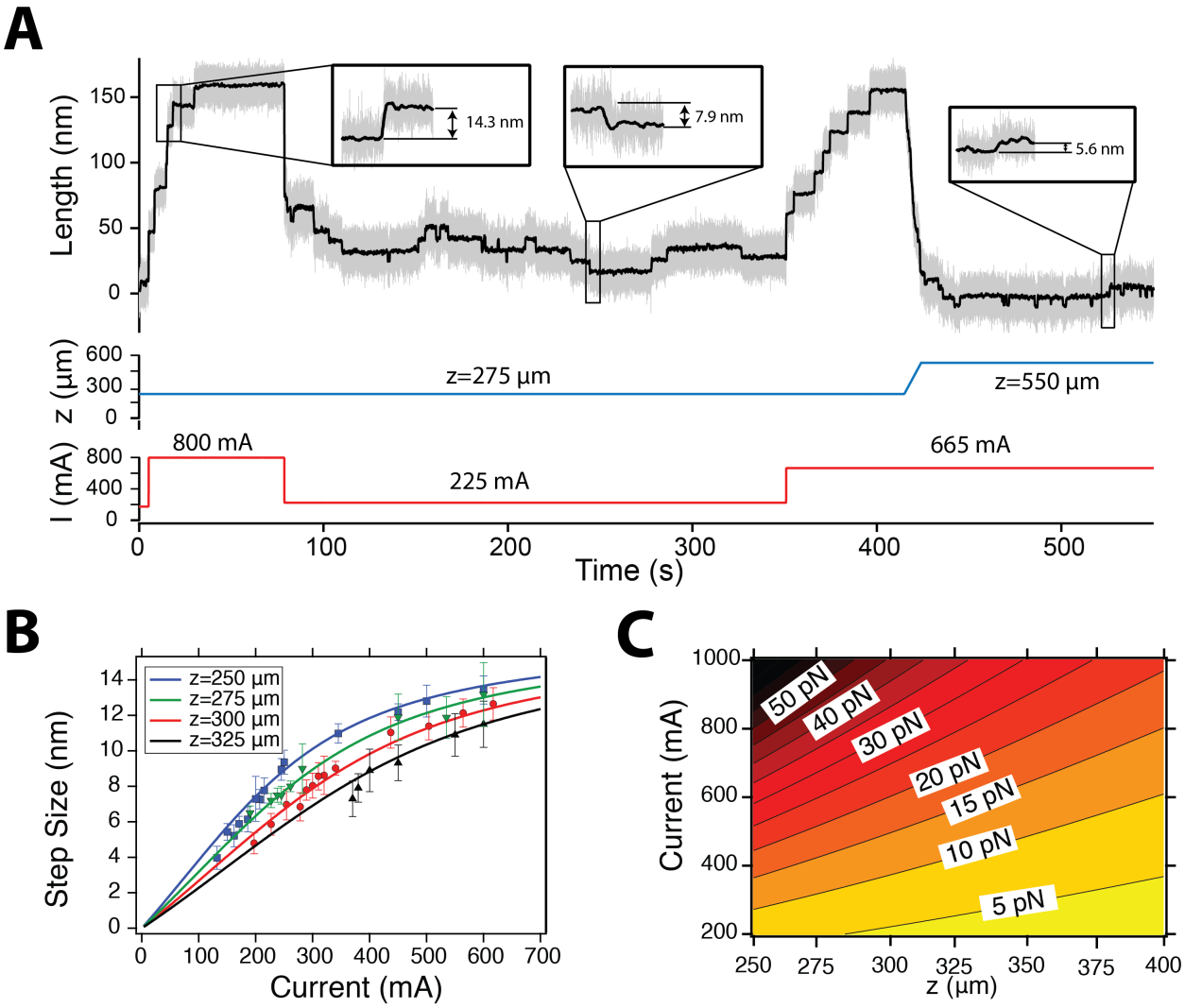

Figure 2: Calibration of the magnetic head tweezers. (A) Protein L dynamics probed at different values of the electric current and distances. The step-sizes scale with the pulling force following the freely jointed chain model, and are used to calibrate our instrument. (B) Step-sizes as a function of the electric current measured at four different distances. Global fit of Eq. (3) to the experimental data yields $A = 0.386 \pm 0.131$ and $B = 9.462 \pm 1.564$, providing the current law. (C) Contour plot of the pulling force applied by the magnetic head to the superparamagnetic beads as a function of the vertical distance z and supplied current I.

force, as the protein readily folds to a state where all eight domains are folded on average, showing steps of 5.6 nm. For each (z, I) condition, we determine the step-sizes as the distance between two consecutive length histograms, calculated over the smoothed trajectory.

Following this strategy, we measure folding/unfolding steps of protein L at distances between 250 μm and 325 μm, and currents between 200 and 1000 mA. The magnetic head saturates when the current reaches 1200 mA, so we can cautiously assume a linear relation between the field and the current below 1000 mA (range over which Karlqvist approximation holds). Figure 2B shows the step sizes measured at four different distances, and plot as a function of the electric current I. Experimental data is globally fit to Eq. 4 through A and B as only free parameters using the Levenberg-Marquardt least orthogonal distance method, with a confidence level of 95%, yielding $A = 0.386 \pm 0.131\ pN/mA^2$ and $B = 9.462 \pm 1.564\ pN/mA$. The fit was weighted with the standard deviation of the distribution of step-sizes. Thus, we establish our current law to be:

$$F(z, I) = 0.386 I^2 \tan^{-1}\left(\frac{12.5}{z}\right) \frac{1}{1 + \left(\frac{z}{12.5}\right)^2} + 9.462 I \frac{1}{1 + \left(\frac{z}{12.5}\right)^2}, \tag{5}$$

since $g = 25$ μm. Equation 5 reveals that the dependence of the pulling force with the distance changes over a length scale of the size of the gap ~ 25 μm. This illustrates the need of positioning the magnetic head with μm precision, since any error in accurately establishing z, such as a slight tilt of the head relative to the fluid chamber will result in a poor determination of z, and thus of the pulling force F.

We validate Eq. 5 to predict accurately the pulling force by describing the folding/unfolding properties of protein L over a wide range of distances and current values. Below 10 pN, protein L shows a steep decreasing probability of populating the folded state. Above 10 pN, protein L unfolds, and the unfolding rates follow an exponential dependence with the force. Given the sharp force dependence of these observables, we use them to test our calibration, by measuring them with the magnetic head tweezers, and comparing their dependence with that had been previously measured.[8,18] Fig. S1 demonstrates the equivalence between our

current law and the magnet law measured determined using slowly coil driven magnets, verifying the accuracy of Eq. 5 in determining the pulling force.

Figure 2C shows a contour plot of the force versus the distance z and current I, where colors scale from yellow to dark red as force increases. The intrinsic nonlinearity of Eq. 5 reflects on the steep dependence of the force with z and I, which can be used to provide a convenient versatility in the force control of magnetic head tweezers. High forces require working at close distances and high currents, but working at farther distances provides a extremely precise force control, since changes of several tenths of mA can lead to changes in the force of a fraction of pN. Our conventional fluid chamber design—built by sandwiching a laser-cut parafilm design with a top cover glass (see methods SI)— allows working up to distances of about ~ 250 μm, giving a force range of $0 - 50$ pN. This force range can be extended if necessary by using thiner chamber designs, or by using larger beads, since the force scales linearly with the volume of the bead.

We validate our description of the force generated by the magnetic head, by confirming the adequacy of Karlqvist approximation (Eq. 1) to describe the magnetic field created by the head, and of Eq. 2 to predict the magnetic force on a superparamagnetic bead. In order to do so, we use talin domain R3 as a force reporter, given its fine force dependence. Figure 3A shows a trajectory of a talin monomer (see SI for details on the construct) measured with the magnetic head tweezers at three different forces, which highlights its aforementioned force sensitivity. At 8.2 pN, talin has a 80% probability of being folded, which drops to 20% at 9 pN, over a force increment of just 0.8 pN. At 8.7 pN, talin populates the folded and unfolded states with equal probability, and transitions between both states with rates of about ~ 1 s^{-1}. The folding probability can be calculated simply as the relative occupation of both states, calculated from a length histogram of the time series. Figure 3B shows the folding probability of talin domain R3, showing its exquisite force dependence, that spans over a force range of 1 pN, so that slight changes in the force lead to large shifts in the folding probability.

We take advantage of this feature to validate the force dependence of our instrument with z, as described by Eq. 5. Figure 3C shows the electric current necessary to observe a folding probability of 0.5—equivalent to 8.7 pN—at different values of the distance z. This dependence can be described analytically by inverting Eq. 5, and obtaining $I(z)$:

$$I(z) = \frac{-9.462 + \sqrt{89.529 + 1.544F \tan^{-1}\left(\frac{12.5}{z}\right)\left[1 + \left(\frac{z}{12.5}\right)^2\right]}}{0.772 \tan^{-1}\left(\frac{12.5}{z}\right)}, \tag{6}$$

which we plot as the solid black line in Fig. 3C for $F = 8.7$ pN. This prediction follows accurately the experimental data, supporting the use of Karlqvist approximation to describe the magnetic field created by the head, and Eq. 2 for the pulling force.

Finally, we take advantage of the ability of the magnetic head tweezers to change the force instantaneously, and explore the folding pathway of protein L at short timescales. To this aim, we design the protocol depicted in Fig. 4A. After the fingerprint pulse (i), we decrease the force to 10 pN to determine the extension of the unfolded protein at this force value (ii), and subsequently to 1 pN during varying times Δt, ranging from 0.01 s to 10 s (iii). Next, we increase the force to 10 pN again, which is the lowest force at which refolding is not permitted (Fig. 3C) (iv). This allows us to observe purely the unfolding of any structure formed during the quench time Δt with the slowest possible kinetics. Magnetic head tweezers allow tight control of the force even during the few millisecond-long force quenches, which would be impossible with the coil-driven permanent magnets.

Figure 4B highlights the quench pulse for two different durations, $\Delta t = 10$ ms (black) and $\Delta t = 250$ ms (red). The lower panel shows the actual change in force, obtained by measuring the electric current across the magnetic head at a sampling rate of 100 kHz. The stepwise change in force takes less than 100 μs. This value depends on the rate at which we supply current to the head, which is at 70 W with the present implementation. More powerful power supplies can further decrease this time constant, although it is now instantaneous for practical purposes, given our sampling rate of ~ 1.5 kHz. When we quench only for 10 ms

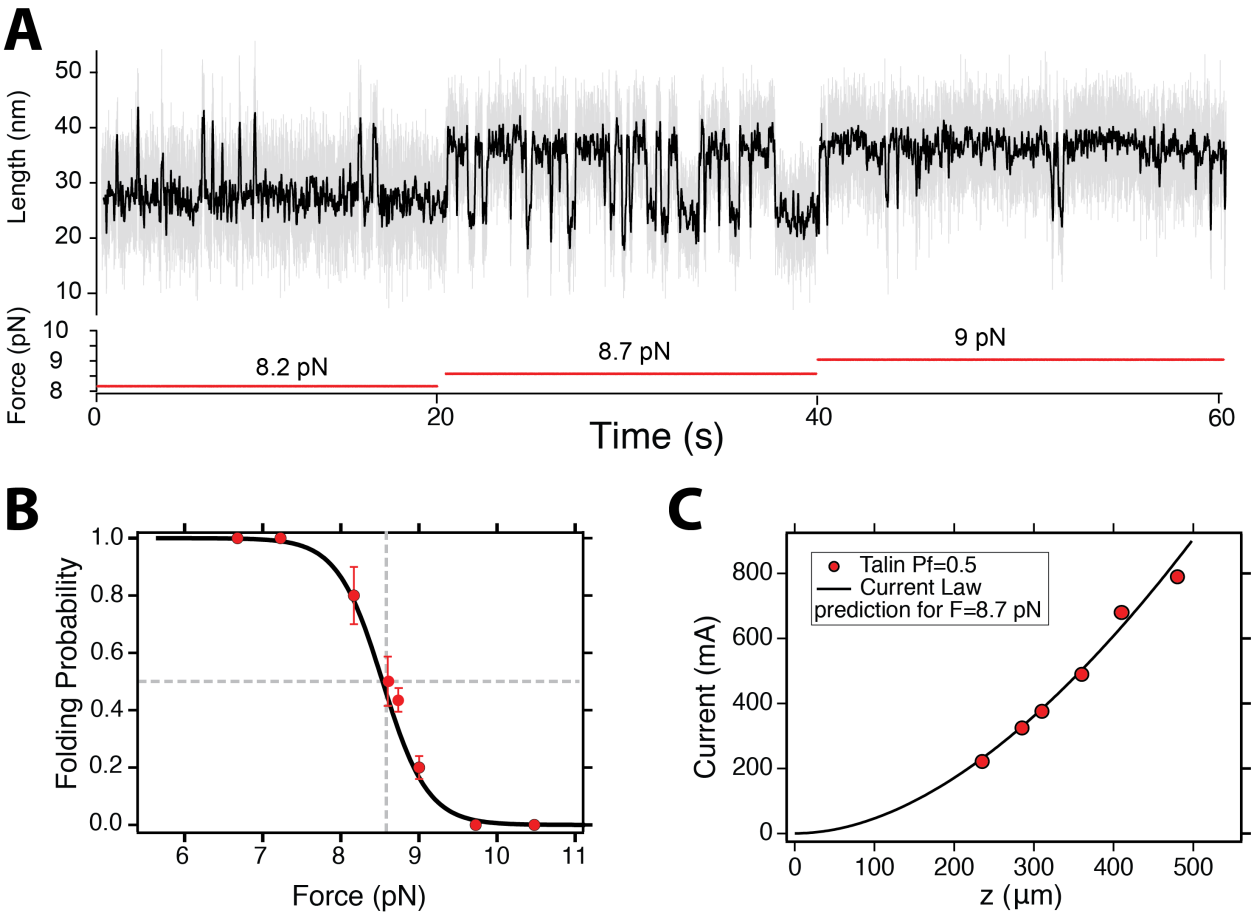

Figure 3: Validation of the current law. (A) Typical talin domain R3 trajectory at three different forces, 8.2, 8.7, 9 pN, with respective folding probabilities of 0.8, 0.5, and 0.2 (B) Folding probability of talin measured with the magnetic head tweezers, with the force at which 0.5 is achieved highligheted. (C) Electric current necessary to observe talin dynamics at a folding probability of 0.5 measured at different distances (red symbols). solid black lines shows the analytical prediction by Eq. 5 with F=8.7 pN.

(black trace), the protein does not reach any stable conformation, and the extension reaches the same level at 10 pN. However, as we increase Δt, the protein L domains start folding and we can capture their folding mechanism at very short timescales. The ultra-fast force change allows us to discriminate between two different kinds of events. First, on a millisecond timescale, we observe the unfolding of a set of weak conformations (red arrowheads). Later, in a timescale of seconds, the native structures unfold, shown as the black arrowheads in Fig. 4A, and reflected also in the extension difference at 10 pN in Fig. 4B.

We characterize in detail the folding pathway of protein L and measure the unfolding times of *every* event observed at 10 pN, and plot them as a square-root histogram in Fig. 4 C. This representation of the unfolding kinetics allows for a systematic identification of events occurring at different characteristic times. In logarithmic scale, an exponential distribution—signature of first-order kinetics—is distributed as $g(t) = \exp\left[t - \tau - \exp(t - \tau)\right]$,[19] where the average unfolding time, τ, appears as a single peak, and thus is easily recognizable. The unfolding time distribution of protein L at 10 pN exhibits an evident bimodal shape, with two different timescales separated by nearly two orders of magnitude. Fitting to a double exponential, we segregate the unfolding events in two different groups; a first set of weak domains that unfold on average at $\tau_{MG} = 0.489 \pm 0.006$ s, and a second stable one unfolding on average at $\tau_N = 47.070 \pm 14.512$ s. The histogram ends abruptly at an abscissa value of 4.6, since the 10 pN pulses are set for 100 seconds. However, we can infer its dynamics from the the left side tail of the distribution, where most events concentrate. This timescale separation allows us to discriminate systematically between two kinds of folding structures by setting a threshold time at 2.01 seconds, crossing point of the individual distributions (dashed bar in Fig. 4C). We measure separately the step-sizes of the weak (Fig. 3 D) and stable domains (inset). Weak domains exhibit a broad step-size distribution, while the stable ones show a gaussian distribution centered at 10.5 nm, with few events scattered at higher extensions. However, we can rank nearly 60% of the weak events onto an analogous step-size distribution about 10.5 nm as (solid red line). This suggests that these weak domains correspond to an

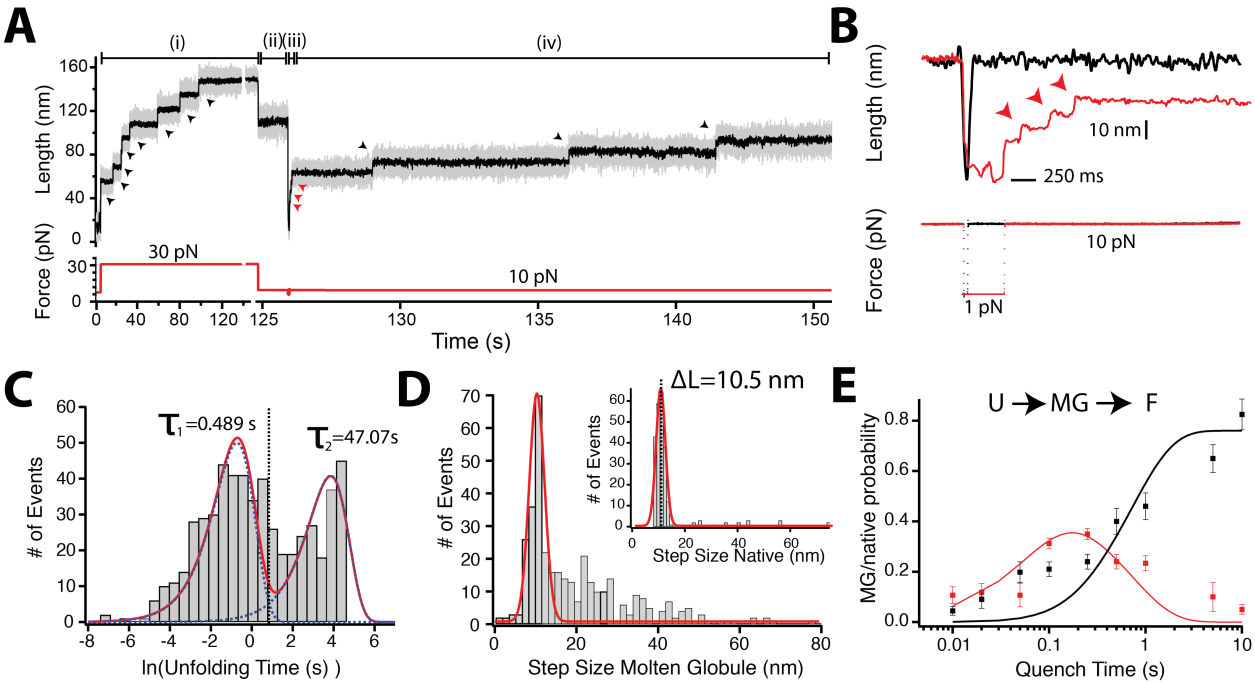

Figure 4: The folding mechanism of protein L upon ultra-fast force quenches. (A) Pulse protocol for characterizing the folding mechanism of protein L. (i) We unfold the protein octamer through a high force pulse (black arrows indicate each unfolding event), (ii) the force is reduced transiently to 10 pN, (iii) then quenched to 1 pN during a varying amount of time Δt; (iv) finally, we probe the folding status of the protein unfolding at low force 10 pN, which readily separates the timescales of the weak domains (red arrows) and native domains (black arrows). (B) Detail of the quench pulse. Black trace shows a quench of $\Delta t = 10$ ms, where the protein does not form the native nor the weak conformation, and thus reaches the same level at 10 pN. In the red trace, we quench during 250 ms, and weak domains are recognized as fast unfolding events (red arrowheads), while native as slow unfolding events, reflected in the extension difference at 10 pN. (C) Square root histograms of the unfolding kinetics of all observed unfolding events at 10 pN. We fit the histogram to a double exponential, which with a logarithmic binning manifests as a bimodal distribution, with each peak associated to a characteristic timescale. The two populations are separated by two orders of magnitude ($\tau_{MG} = 0.489$, and $\tau_N = 47.07$ s), revealing the presence of mechanically weak states. (D) Histogram of the unfolding step sizes of the weak domains (unfolding within less than 2.05 s, and the native states (inset). The immature states show a broad distribution of unfolding lengths, although the large majority unfolds through a step size of ~ 10 nm, as the native ones, suggesting their nature as immature states. (E) Probability of the molten-globule(red) and native states (black) as a function of the quench time Δt. We fit the distributions globally to a first order kinetics model with one intermediate, revealing the kinetics of forming the molten globule ($r_{MG} = 15.24\ s^{-1}$) and the native ($r_N = 1.39\ s^{-1}$).

immature conformation that eventually evolves to the stable native conformation.

We delve into this property and characterize the folding mechanism of protein L as a sequential reaction from the unfolded state (U) to a molten-globule state (MG) that matures eventually to the native conformation (N). These observations are similar to those made previously on ubiquitin using the AFM.[20] However, here they are made on a faster timescale, and with an accurate control of the force in the low range. Figure 4E shows the probability of appearance of the molten globule and native conformations as a function of the quenching time Δt. The molten globule is manifested optimally in a timescale of ~ 100 ms, decaying quickly when we quench during seconds. Oppositely, the native domains show a sigmoid-like behavior, which saturates after few seconds. This dependence can be accurately described by a kinetic model where the molten globule appears as an intermediate of the native conformation (see SI for an explicit derivation of the kinetic model). Solid lines in Fig. 4E show the global fits of the molten globule/native probability as a function of the quench time, which yield the microscopic rates of formation of the molten globule ($r_{MG} = 1.06 \pm 2.22\ s^{-1}$) and the native state ($r_N = 0.51 \pm 0.05\ s^{-1}$). The fraction of native states does not saturate to 1 even when the quench time is of 10 seconds, but rather to a value of 0.85. This is due to the a residual formation of stable non-native conformation with large step sizes (see inset in Fig. 4D), that can be related to domain swap-like structures. These events are corrected when the quench force is higher.

In summary, we have implemented a magnetic head design for force spectroscopy, which enables changing the force with a bandwidth above 10 kHz, while maintaining an accurate control over a large range of pulling forces. We calibrated successfully the instrument by using protein L step-sizes, and taking advantage of the framework of magnetic recording theory to describe analytically the pulling force as a function of the electric current and the vertical distance from the head to the bead. Using the magnetic head tweezers, we described the folding mechanism of protein L at very short timescales, demonstrating the existence of a molten globule state which forms in few milliseconds, and thus would be otherwise hidden in

the force change lag time introduced by most force spectrometers. Magnetic head tweezers open the possibility of novel force protocols, more complex than simple stepwise changes in the pulling force. Force spectroscopy has traditionally been used to infer the folding status of proteins, or to test the mechanical stability of proteins; this is, to investigate how do proteins respond to the *magnitude* of the pulling force. However, it is generally unexplored how fast can proteins respond to forces which change in time, or, in other words, how do they respond to the spectral density of a force signal. Mechanical forces in physiology are unlikely to consist of simple protocols such as constant or ramped forces. For instance, the cellular environment is extremely noisy. Yet, cellular force sensors are capable to recognize and respond effectively to mechanical information amongst the environmental noise.[21,22] Also, it appears essential to explore how biomolecules interact with force signals which cycle in time at different frequencies, being this the sort of perturbations typically recognized in a number of physiological examples, such as the auditory system, heart beating, or cellular locomotion.[23–25] We envision that the potentiality of magnetic head tweezers will be able to address these problems by recreating mechanical perturbations which mimic those encountered in physiology, and thus to open a range of unquestioned biological problems.

References

(1) Buschow, K.; Long, G.; Grandjean, F. *High Density Digital Recording*; Springer Netherlands, 1993; Vol. 229.

(2) Mallinson, J. C. *The Foundations of Magnetic Recording*; Academic Press, 1993.

(3) Vlaminck, I. D.; Dekker, C. Recent Advances in Magnetic Tweezers. *Annual Review of Biophysics* **2012**, *41*, 453–472, PMID: 22443989.

(4) Gosse, C.; Croquette, V. Magnetic Tweezers: Micromanipulation and Force Measurement at the Molecular Level. *Biophysical Journal* **2002**, *82*, 3314–3329.

(5) Lipfert, J.; Hao, X.; Dekker, N. H. Quantitative Modeling and Optimization of Magnetic Tweezers. *Biophysical Journal* **2009**, *96*, 5040–5049.

(6) Popa, I.; Rivas-Pardo, J. A.; Eckels, E. C.; Echelman, D. J.; Badilla, C. L.; Valle-Orero, J.; Fernandez, J. M. A HaloTag Anchored Ruler for Week-Long Studies of Protein Dynamics. *Journal of the American Chemical Society* **2016**, *138*, 10546–10553, PMID: 27409974.

(7) Kemmerich, F. E.; Swoboda, M.; Kauert, D. J.; Grieb, M. S.; Hahn, S.; Schwarz, F. W.; Seidel, R.; Schlierf, M. Simultaneous Single-Molecule Force and Fluorescence Sampling of DNA Nanostructure Conformations Using Magnetic Tweezers. *Nano Letters* **2016**, *16*, 381–386.

(8) Valle-Orero, J.; Rivas-Pardo, J. A.; Tapia-Rojo, R.; Popa, I.; Echelman, D. J.; Haldar, S.; Fernandez, J. M. Mechanical Deformation Accelerates Protein Ageing. *Angewandte Chemie International Edition* **2017**, *56*, 9741–9746.

(9) Popa, I.; Berkovich, R.; Alegre-Cebollada, J.; Badilla, C. L.; Rivas-Pardo, J. A.; Taniguchi, Y.; Kawakami, M.; Fernandez, J. M. Nanomechanics of HaloTag Tethers. *Journal of the American Chemical Society* **2013**, *135*, 12762–12771, PMID: 23909704.

(10) Haldar, S.; Tapia-Rojo, R.; Eckels, E. C.; Valle-Orero, J.; Fernandez, J. M. Trigger factor chaperone acts as a mechanical foldase. *Nature Communications* **2017**, *8*, 668.

(11) Karlqvist, O. *Calculation of the magnetic field in the ferrowmagnetic layer of a magnetic drum*; Transactions of the Royal Institute of Technology, Stockholm, Sweden; Goterborg, Elanders boktr, Stockholm, 1954.

(12) Yao, M.; Goult, B. T.; Chen, H.; Cong, P.; Sheetz, M. P.; Yan, J. Mechanical activation of vinculin binding to talin locks talin in an unfolded conformation. *Scientific Reports* **2014**, *4*, 4610 EP –.

(13) Yao, M.; Goult, B. T.; Klapholz, B.; Hu, X.; Toseland, C. P.; Guo, Y.; Cong, P.; Sheetz, M. P.; Yan, J. The mechanical response of talin. *Nature Communications* **2016**, *7*, 11966 EP –.

(14) Fisher, J. K.; Cribb, J.; Desai, K. V.; Vicci, L.; Wilde, B.; Keller, K.; Taylor, R. M.; Haase, J.; Bloom, K.; O'Brien, E. T.; Superfine, R. Thin-foil magnetic force system for high-numerical-aperture microscopy. *The Review of scientific instruments* **2006**, *77*, 023702–1–023702–9.

(15) Janssen, X. J. A.; Lipfert, J.; Jager, T.; Daudey, R.; Beekman, J.; Dekker, N. H. Electromagnetic Torque Tweezers: A Versatile Approach for Measurement of Single-Molecule Twist and Torque. *Nano Letters* **2012**, *12*, 3634–3639.

(16) Doi, M.; Edwards, S. *The Theory of Polymer Dynamics*; Oxford Science Publications, 1986.

(17) Shevkoplyas, S. S.; Siegel, A. C.; Westervelt, R. M.; Prentiss, M. G.; Whitesides, G. M. The force acting on a superparamagnetic bead due to an applied magnetic field. *Lab Chip* **2007**, *7*, 1294–1302.

(18) Valle-Orero, J.; Tapia-Rojo, R.; Eckels, E. C.; Rivas-Pardo, J. A.; Popa, I.; Fernandez, J. M. Proteins Breaking Bad: A Free Energy Perspective. *The Journal of Physical Chemistry Letters* **2017**, *8*, 3642–3647, PMID: 28723106.

(19) Sigworth, F. J.; Sine, S. M. Data transformations for improved display and fitting of single-channel dwell time histograms. *Biophys J* **1987**, *52*, 1047–1054.

(20) Garcia-Manyes, S.; Dougan, L.; Badilla, C. L.; Brujić, J.; Fernandez, J. M. Direct observation of an ensemble of stable collapsed states in the mechanical folding of ubiquitin. *Proceedings of the National Academy of Sciences* **2009**, *106*, 10534–10539.

(21) Johnson, H. Thermal noise and biological information. *Q. Rev. Biol.* **1987**, *62*, 141–152.

(22) Tsimring, L. S. Noise in Biology. *Reports on progress in physics. Physical Society (Great Britain)* **2014**, *77*, 026601–026601.

(23) Yusko, E. C.; Asbury, C. L. Force is a signal that cells cannot ignore. *Molecular Biology of the Cell* **2014**, *25*, 3717–3725.

(24) Salvi, J. D.; Ó Maoiléidigh, D.; Fabella, B. A.; Tobin, M.; Hudspeth, A. J. Control of a hair bundle's mechanosensory function by its mechanical load. *Proceedings of the National Academy of Sciences* **2015**, *112*, E1000–E1009.

(25) Kronenberg, N. M.; Liehm, P.; Steude, A.; Knipper, J. A.; Borger, J. G.; Scarcelli, G.; Franze, K.; Powis, S. J.; Gather, M. C. Long-term imaging of cellular forces with high precision by elastic resonator interference stress microscopy. *Nature Cell Biology* **2017**, *19*, 864 EP –.